Quantification of extra virgin olive oil adulteration using smartphone videos

Weiran Song [a, 1], Zhiyuan Song [b, 1], Jordan Vincent [c], Hui Wang [c, *], Zhe Wang [a]

[a] *State Key Lab of Power System, Department of Energy and Power Engineering, Tsinghua University, Beijing, 100084, China*
[b] *Department of Engineering, King's College London, Strand, London, England, WC2R 2LS, UK*
[c] *School of Computing, Ulster University, Newtownabbey, Co. Antrim, BT37 0QB, UK*

* Corresponding author.
E-mail address: h.wang@ulster.ac.uk (H. Wang).
[1] These authors contributed equally to this work.

Abstract

Edible oil adulteration is a main concern for consumers. This paper presents a study on the use of smartphone, coupled with image processing and chemometrics, to quantify adulterant levels in extra virgin olive oil. A sequence of light with varying colours is generated on the phone screen, which is used to illuminate oil samples. Videos are recorded to capture the colour changes on sample surface and are subsequently converted into spectral data for analysis. To evaluate the performance of this video approach, partial least squares regression models constructed from such video data as well as near-infrared, ultraviolet-visible and digital imaging data are compared in the task of quantifying the level of vegetable oil in extra virgin olive oil in the range 5%−50% (v/v). The results show that the video approach (R^2 = 0.98 and RMSE = 0.02) yields comparable performance to baseline spectroscopy techniques and outperforms computer vision system approach. Since the smartphone-based sensor system is low-cost and easy to operate, it has high potential to become a consumer-oriented solution for detecting edible oil adulteration.

Keywords: Olive oil adulteration; Smartphone video; NIR; UV-Vis; Computer vision; Chemometrics

1. Introduction

Extra virgin olive oil (EVOO), known as liquid gold, is a high-priced product of great nutritional value. It provides a good source of monounsaturated fatty acids, vitamins, antioxidants and phenolics, which is often associated with the prevention of health problems, such as obesity, diabetes, atherosclerosis, heart disease, high blood pressure and cancer [1][2]. Due to the high price and increasing demand of olive oil [3], olive oil adulteration where it is mixed with less expensive edible vegetable oils (VO) becomes a serious food fraud issue that reduces consumer confidence, ruins brand reputation and causes health problems.

Well-preserved pure EVOO and VO can be easily separated by trained eyes because EVOO is richer in pigments such as chlorophylls and carotenoids compared to VO [4][5]. However, it is difficult for consumers to assess the level of VO adulteration in EVOO based on sensory analysis. Traditional techniques such as mass spectrometry [6], gas/liquid chromatography [7] and nuclear magnetic resonance spectroscopy [8] have been frequently used for quality control of olive oil. Although these methods are powerful and sensitive enough to assess the level of

adulteration, most of them are expensive, time consuming, and require cumbersome sample preparation. Therefore, novel techniques which can quantify olive oil adulteration in a cost-effective, quick and non-destructive way is desperately desired by food industry and consumers.

A state-of-the-art technique that has been successfully applied in food authentication and quality assessment is spectroscopy. It measures the interaction between chemical compounds and radiated light wavelengths using near infrared (NIR), ultraviolet-visible (UV-Vis), Raman, fluorescence and Fourier transform-infrared (FT-IR) spectrometers [9][10][11]. The obtained spectra contain useful fingerprint information and are represented as sets of light intensity values at varying wavelengths. Spectroscopy coupled with chemometrics provides a highly efficient way for the qualitative and quantitative analysis of olive oil properties, including provenance, mineral composition and adulterant level [5][11][12]. Specifically, the use of portable spectrometer even presents comparable results to traditional approaches in detecting olive oil adulteration. For example, Raman spectroscopy coupled with least squares support vector machine (LS-SVM) obtains 0.9976 of R^2 value in predicting adulterant level ranging from 0% to 100% (v/v) at 10% increments [13]. Such a result is comparable to that of using gas chromatography in measuring similar adulterant level [14]. Another technique recently used for food authentication is computer vision system (CVS) [15]. It aims to replace human visual system by soft sensor and automatically gain high-level understanding of food quality through image acquisition, processing and analysis. CVS has been reported to perform well in detecting olive oil adulteration because it can effectively capture the colour level difference between olive oil and adulterated oil [16]. A brief overview of using the above techniques and chemometrics for detecting olive oil adulteration is presented in **Table S1** (see Supplementary Materials).

Although spectroscopy is a powerful tool in authentication of olive oil, its high cost still exceeds consumer expectation. For example, the price of a portable NIR spectrometer (NIRQuest512, Ocean Optics) is around 15600 USD. Recent technology attempts to minimize the size and price of spectrometer, yielding pocket sized spectrometers such as SCIO and TellSpec [17][18]. These spectrometers can help consumers to assess food quality in a quick and convenient way when connected to a smartphone. However, the price of such hardware is still high, ranging from 950 to 1899 USD. CVS is not an appropriate method for consumers to use to detect olive oil adulteration as it requires careful setting of camera, well-defined and consistent illumination [15]. Moreover, conventional CVS needs an external camera and computer software to acquire and process image respectively. Such instrumental limitation prevents data from being obtained and analysed instantaneously. Recent studies attempt to use mobile devices such as smartphone to replace external camera for food authentication and quality assessment [19]. Consumers can upload photos to the smartphone application or cloud servers and then obtain real-time analytical results of food products.

Our previous work proposed a sensor system that uses smartphone videos and pattern recognition for food authentication [20]. Spectral information was captured under coloured illuminations and processed by computer vision techniques. This sensor system coupled with locally weighted partial least squares classification (LW-PLSC) obtained over 95% of classification accuracies in authenticating olive oil sampled under variable conditions. However, the use of smartphone videos for olive oil authentication still requires further investigation. On one hand, the quantitative research of using smartphone videos to detect olive oil adulteration has not been

studied, including the regression performance of low-cost video data and the minimum concentration of adulterated oil that can be effectively identified by the sensor system. If the adulterant degree can be successfully determined by way of data regression, consumers can easily assess the purity of olive oil via a smartphone. On the other hand, the performance comparison between the video approach and baseline methods such as spectroscopy and CVS has not been investigated. The hardware for video acquisition is limited to the visible wavelength range (around 380−740 nm), which is narrower than the wavelength range of UV-Vis (190−780 nm) and NIR (780−2500nm) spectrometers. Therefore, it is worthy of investigating if the video approach can achieve performance comparable to UV-Vis and NIR spectroscopy when detecting certain level of olive oil adulteration. Compared to a well-defined and consistent illumination in CVS experimental setup, the light of our sensor system is generated by smartphone screen in a less controlled environment. Nevertheless, our sensor system contains the spectral information that CVS does not have. This leads to a question: will the video approach perform better than CVS on the same detection task given that the sampling condition and camera are similar? Furthermore, our previous work did not provide a comprehensive interpretation on how variables contribute to the model used for detection/quantification of olive oil adulteration. The selection of important variables can reduce the computational time and the memory usage, thereby improving the efficiency of the video approach as a real-time system.

This paper aims to quantify the adulteration levels of VO in EVOO by using a low-cost approach and compare its performance with several baseline methods. For this purpose, sample videos were recorded via a smartphone and converted into colour spectra by image processing techniques. Baseline experiments were implemented on the same samples using three methods, including CVS, NIR and UV-Vis spectrometers. Results obtained from PLS regression were compared in terms of the root-mean-square error (RMSE) and the coefficient of determination (R^2). Furthermore, a variable selection process was carried out and its effect on the performance of PLS regression models was evaluated.

2. Material and Methods

2.1. Samples

To prepare the samples, two oils were purchased from a Tesco supermarket in Northern Ireland in August of 2019: EVOO (product of Italy) and rapeseed oil (product of more than one country). The oils were within their best before date and were stored in a dry and dark place at room temperature to avoid degradation as much as possible. A total of 77 samples were prepared, including 7 pure EVOO samples and 70 adulterated samples in ten different concentrations from 5% to 50% (v/v) at an increment of 5%. Each sample was 20mL in volume, placed in plastic shot glasses (approximately 30mL), manually shaken for about 30s and scanned by smartphones, NIR and UV-Vis spectrometers.

2.2. Video sensor system

A sensor system based on smartphone videos was investigated to quantify the adulteration of EVOO with VO by extracting and analysing colour spectral information. A smartphone (Samsung Galaxy S6) was used to generate a sequence of colours on its screen varying from purple to red and illuminate oil samples. To ensure a uniform illumination on sample surface, the smartphone was parallelly placed about 5cm from the sample surface, with the centre of screen facing the sample surface. A 5-second video of 32-bit and 960× 720 pixels was recorded by front camera (5MP and f/1.9 aperture) and stored in MP4 format with file size of approximately 7MB. Two sets of sampling were conducted in laboratory under ambient light (6pm) and low-light (10pm) conditions, with each set lasting approximately 50 minutes for 77 samples.

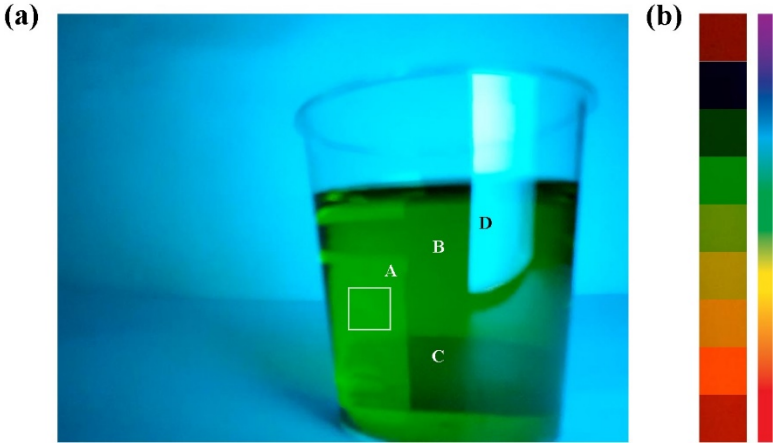

Fig. 1. (a) The 50th frame of a smartphone video. Oil sample was illuminated using smartphone screen (cyan colour) and the selected ROI with 70 × 70 pixels was marked in a white square; (b) a subset of ROI images and a sequence of colours varying from purple to red.

The obtained videos were uploaded to a laptop computer installed with MATLAB 7.12 R2011a software (The MathWorks Inc., USA) for image processing and data analysis. Each video was automatically split into 175 or 176 frames (images) and only the first 175 frames were used in the selection of region of interest (ROI). The 50th frame in a video is shown in Fig. 1a, where an oil sample was illuminated using smartphone screen with cyan colour. We divide the sample into 4 regions with uniform colour levels and sufficient areas. Region A contains a selected ROI with 70 × 70 pixels (a white square) which presents the real colour level of sample under illumination. Region B and C are darker than region A because multiple factors such as container and background can cause shadows and refraction. Region D has the same colour as screen illumination due to the reflection. If ROI is respectively selected from region A to D, the corresponding quantification performance will gradually decrease. The same size of ROI is manually selected for all sample videos in region A to prevent ROI contains noisy colours. Fig. 1b shows a subset of ROI images in which the colour illumination changes from purple to red. The ROI images were then decomposed according to red (R), green (G) and blue (B) colour channels with colour levels varying from 0 to 255. By averaging the colour level of an ROI image, the colour spectral information for each sample was represented as a 525-dimensional vector (175 frames × 3 colour channels).

2.3. Baseline methods

2.3.1 NIR spectroscopy

A portable NIR spectrometer (NIRQuest512, Ocean Optics, Inc., USA) equipped with an InGaAs detector was used to obtain spectra in absorbance mode, ranging from 901.06 to 1721.242 nm with a spectral resolution of 1.65 nm. The experiment was conducted under ambient light condition at room temperature. A 45° diffuse reflectance probe (DR-Probe) with integrated tungsten halogen light source was used for illumination. The NIR spectral data of 512 variables was acquired with the OceanView software. Each sample was scanned for 5 times within 5 seconds and the average spectrum was used as a data sample.

2.3.2 UV-Vis spectroscopy

Absorbance spectra with wavelength ranging from 185.5 to 666.082 nm (1.5 nm interval) were collected by a UV-Vis spectrometer (STS UV-Vis, Ocean Optics, Inc., USA). The same DR-Probe was used for illumination and each sample was recorded for 5 times within 25 seconds under ambient light condition at room temperature. An average spectrum with 1080 variables was obtained by the OceanView software for further analysis.

2.3.3 Digital imaging

A smartphone (Huawei P30 Pro) with high-performance front camera (32MP and f/2.0 aperture) was used to acquire 24-bit digital images with 6528 × 4896 pixels spatial resolution. The image acquisition process was conducted inside a compartment in order to reduce the influence of external light and maintain the uniformity of illumination. The camera was fixed 5cm away from the sample and acquired images twice through plastic glasses under ambient light and LED illumination conditions. The obtained image was stored in JPEG format with file size of approximately 3.7MB. **Fig. S1** shows ROI images (200 × 200 pixels) of pure EVOO, EVOO adulterated with VO at different levels and pure VO. The colour difference between EVOO and VO is significant, however, the level of VO in mixed oil cannot be effectively identified by naked eyes. To quantify the level of adulteration, each ROI image was decomposed into three images based on RGB channels with colour levels varying from 0 to 255. The frequencies of colour levels were calculated for each channel, resulting in three histograms and a data vector with 768 variables (256 colour levels × 3 colour channels). The data matrix was then constructed by samples and variables located in rows and columns, respectively.

2.4. Data analysis

The obtained dataset for each instrumentation was split into a calibration set and an independent test set according to the ratio of 5:2. To maintain the same diversity in both sets, DUPLEX algorithm [21] was applied to samples of the same adulteration level. Regression model based on the calibration set was optimised by leave-one-out cross-validation and then tested on samples from the test set.

The video, spectral and image data were fed to chemometrics methods to investigate the relationship between input variables and adulteration levels. These data are usually high-dimensional and multicollinear that the regression coefficient of ordinary least squares is instable and calculated inefficiently. PLS regression is a standard method for analysing high-dimensional and multicollinear data in chemometrics, which relies on the basic assumption that the investigated system or process is driven by a set of underlying latent variables (LVs). It searches for linear combinations of predictor variables **X** that maximize the covariance between the LV and the response **y**. This procedure is iteratively conducted using deflation scheme to ensure the mutual orthogonality of the LVs. We adopt nonlinear iterative partial least squares (NIPALS) algorithm [22] for PLS calculation which is summarized in Table 1.

Table 1. The PLS algorithm.

Input	Predictor variables **X**
	Response **y**
	The number of latent variables *k*
Output	**T** (**X**-score matrix)
	P (**X**-loading matrix)
	q (**y**-loading vector)
	PLS regression coefficients **b**
Step *1*	Compute the loading weights: $\mathbf{w} = \mathbf{X}^T \mathbf{y}$
Step *2*	Normalize the weights: $\mathbf{w} = \mathbf{w} / \|\|\mathbf{w}\|\|$
Step *3*	Compute the score of **X**: $\mathbf{t} = \mathbf{X}\,\mathbf{w}$
Step *4*	Compute the loading vector of **X**: $\mathbf{p} = \mathbf{X}^T \mathbf{t} / (\mathbf{t}^T \mathbf{t})$
Step *5*	Compute the loading vector of **y**: $\mathbf{q} = \mathbf{y}^T \mathbf{t} / (\mathbf{t}^T \mathbf{t})$
Step *6*	Deflate **X** and **y**: $\mathbf{X} = \mathbf{X} - \mathbf{t}\,\mathbf{p}^T$, $\mathbf{y} = \mathbf{y} - \mathbf{t}\,q$
Step *7*	Store **w**, **t**, **p** and *q* in **W**, **T**, **P** and **q** respectively
Step *8*	Return to step *1* until reaching *k* latent variables
Step *9*	Compute the regression coefficients: $\mathbf{b} = \mathbf{W}^T (\mathbf{P}\mathbf{W}^T)^{-1} \mathbf{Q}$

In this work, the maximum number of LVs in PLS regression is set to 8 to prevent overfitting. Variable importance in projection (VIP) is a popular variable selection method which accumulates the importance of each variable being reflected by the loading weights **w** from each LV [23]. The VIP score of the *j*-th variable is defined as:

$$VIP_j = \sqrt{M \sum_{k=1}^{K} (w_{jk}^2 q_k^2 (\boldsymbol{t}_k^T \boldsymbol{t}_k) / ||\boldsymbol{w}_k^2||) \,/\, \sum_{k=1}^{K} q_k^2 (\boldsymbol{t}_k^T \boldsymbol{t}_k)} \quad (1)$$

where *M* is the number of variables and *K* is the number of LVs in PLS model. Generally, a variable should be selected if its VIP score is above 1, but a proper threshold above 0.8 is frequently used and can yield more relevant variables.

To assess the accuracy of regression models, the coefficient of determination and the root-mean-square errors of calibration (R^2_C and RMSEC), cross-validation (R^2_{CV} and RMSECV) and prediction (R^2_P and RMSEP) are calculated as follows:

$$R^2 = 1 - \frac{\sum_{i=1}^{N} (\hat{y}_i - y_i)^2}{\sum_{i=1}^{N} (\hat{y}_i - \bar{y})^2} \quad (2)$$

$$RMSE = \sqrt{\frac{\sum_{i=1}^{N}(\hat{y}_i - y_i)^2}{N}} \quad (3)$$

where N is the number of samples, $\hat{y}_i$ is the predicted value of the i-th sample, y_i is the reference value of the i-th sample, $\bar{y}$ is the average value of response. Generally, high R^2 and low RMSE values indicate that the regression models are well-performing.

3. Results and discussion

3.1. Video, spectral and image data

Two sets of video data obtained under ambient light (a) and low-light (b) conditions are shown in Fig. 2. The video data has 525 variables in RGB colour channels and are averaged according to the levels of VO for better visualization. For each channel, variables with large numerical values indicates that its corresponding ROI image has a similar colour to the channel colour. A clear distinction between the averaged samples belonging to the different VO levels can be found in specific variable ranges, such as variables 100−150 for set-a and variables 240−280 for set-b. In these intervals, samples with high VO levels usually has larger values than samples with low VO levels. As the two sets of data present a significant difference in spectral shape and colour levels, the regression model based on one set is inefficient when predicting data from another set due to the restricted applicability domain [24]. The two sets of data are further plotted according to the principal component analysis (PCA) scores (see Fig. 3), which clearly present different levels of adulteration. The first two principal components accumulate 79.9% and 52.6% of the total variance for two sets, respectively.

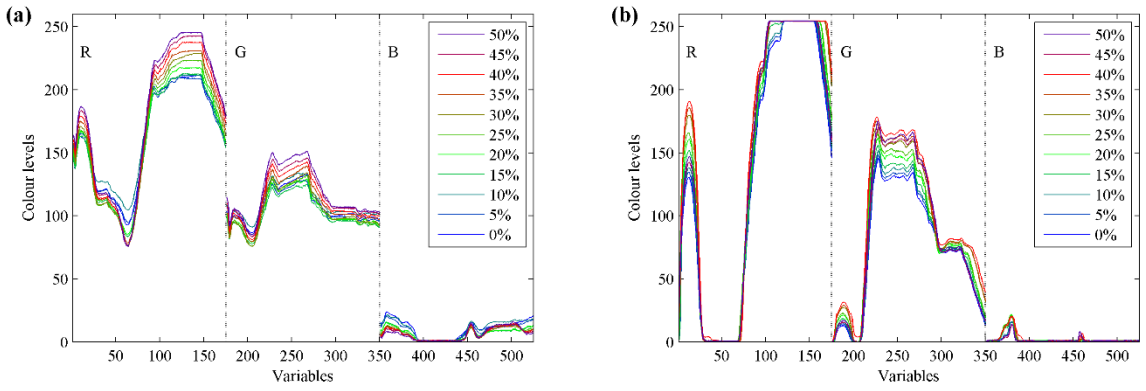

Fig. 2. Average video data of non-adulterated and adulterated EVOO samples collected under ambient light (a) and low-light conditions (b). Variables 1-175, 176-350 and 351-525 belongs to red, green and blue colour channels, respectively.

The raw and pre-processed NIR spectra of 77 oil samples are respectively shown in **Fig. S**2a and b. The distinction between samples having different VO levels cannot be visually perceived due to the scattering effects. We investigate several pre-processing techniques as well as their combinations to correct the baseline difference and improve prediction performance. These techniques include standard normal variate (SNV), spectrum conversion (SC) from absorbance to transmittance, Savitsky-Golay (SG) smoothing and first derivative. The SG filter using

second-order polynomial has a window width ranging from 5 to 25 with an increment of 2. After pre-processing, the averaged EVOO and VO data are shown in **Fig. S**2c where the two samples can be distinguished around the wavelength 1200nm. **Fig. S**3 shows the raw (a) and pre-processed (b) UV-Vis data. The same pre-processing techniques are investigated on the raw data. The averaged EVOO and VO samples present a clear distinction, especially after wavelength 570 nm, as shown in **Fig. S**3c. The PCA scatter plots of the NIR and UV-Vis data can be found in **Fig. S**4, where the UV-Vis data is more discriminative at the adulteration levels than NIR data. The main results of NIR and UV-Vis spectral data pre-processing will be given in Section 4.2.

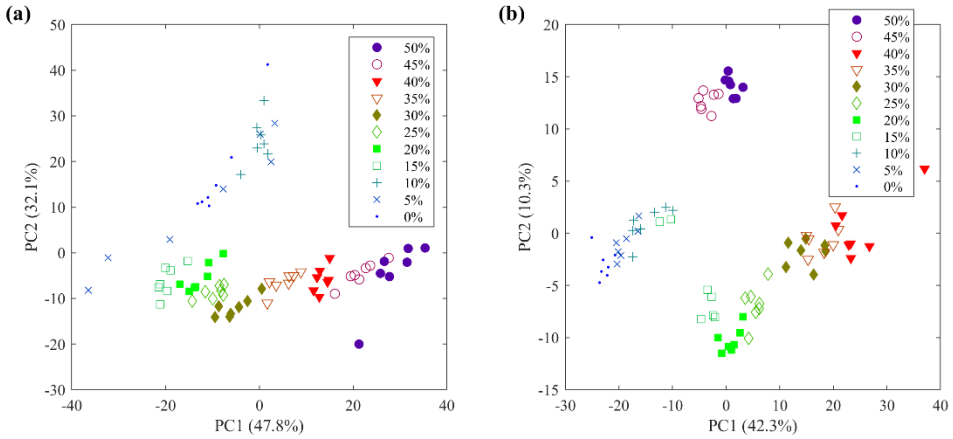

Fig. 3. PCA scatter plot of the video data using first two principal components: data collected under ambient light (a) and low-light (b) conditions.

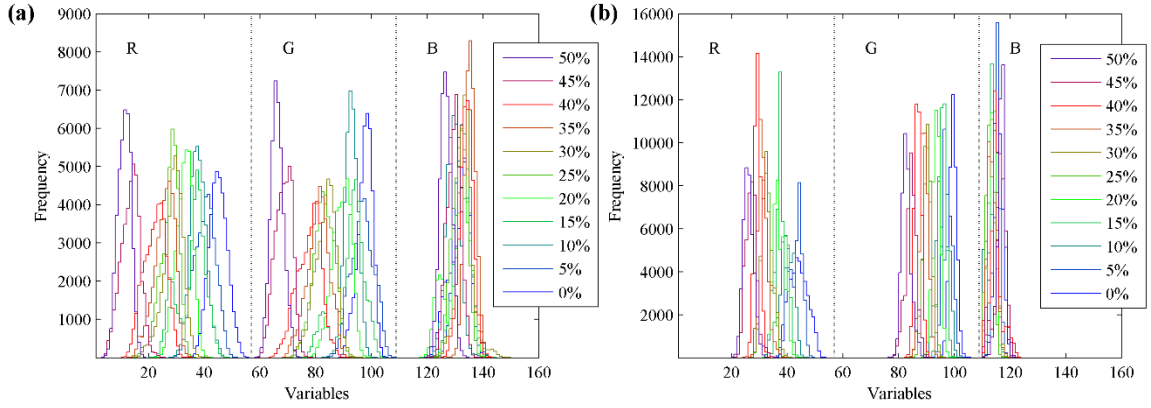

Fig. 4. Average histograms of EVOO samples adulterated with different levels of VO. Two sets of image data were respectively collected under ambient light (a) and low-light conditions (b).

Two sets of oil image data collected in ambient light (a) and low-light (b) environments are depicted as RGB histograms. The non-informative columns with zero values were removed from the image data, resulting in 145 and 86 variables for two sets, respectively. Samples are averaged according to the levels of VO for better visualization as shown in Fig. 4. The difference between the averaged data with varying VO concentrations mainly occurs in red and green colour channels. With the decrease of VO concentrations, the peak (highest frequency) of eleven samples mostly shifts from low numbers of variables to high numbers of variables in red and green colour channels. It indicates that the decomposed colour of the samples having low adulteration levels tends to be red or

green. However, the frequencies of histograms do not appear in the same way for two sets due to the inconsistent sampling environments. The PCA scatter plots of the NIR and UV-Vis data can be found in **Fig. S5**.

3.2. Quantitative analysis

The main results of PLS regression model on the raw and pre-processed data from NIR and UV-Vis spectroscopy are presented in Table 2. The three parameters in SG filter function are window width, polynomial order and derivative order (0: smoothing), respectively. The model based on raw NIR data has a poor performance ($RMSE_{CV}$ = 0.0681, R^2_{CV} = 0.8147, $RMSE_P$ = 0.053 and R^2_P = 0.8878) due to the scattering effects. The baseline difference is efficiently corrected after normalization, resulting in a significant improvement of R^2 (~0.929) in validation and prediction. If the absorbance spectra are converted into transmittance spectra, the results of R^2 can be further improved by over 3%. Data smoothing reduces the $RMSE_{CV}$ to some extent, however it may be at the risk of increasing $RMSE_P$. The model based on raw UV-Vis spectra can quantify the adulterant level with high efficiency ($RMSE_{CV}$ = 0.0168, R^2_{CV} = 0.9887, $RMSE_P$ = 0.0123 and R^2_P = 0.994). The SNV normalization slightly improves the performance measurements, while smoothing and the first derivative will not significantly improve the PLS regression model.

Table 2. Performance measurements of PLS regression model for the prediction of VO concentration, using raw and pre-processed data from NIR and UV-Vis spectroscopy.

	Pre-processing	LVs	$RMSE_{CV}$	R^2_{CV}	$RMSE_P$	R^2_P
NIR	Raw	8	0.0681	0.8147	0.053	0.8878
	SNV	8	0.042	0.9295	0.0421	0.9292
	SG (17,2,1)	8	0.0663	0.8244	0.054	0.8835
	SG (17,2,1) + SNV	8	0.0362	0.9475	0.0459	0.9156
	SNV + SC	8	0.0298	0.9646	0.0212	0.9819
	SNV + SG (11,2,0) + SC	8	0.0256	0.9738	0.0253	0.9744
	SNV + SC + SG (9,2,0)	8	0.0263	0.9724	0.0245	0.9759
UV-Vis	Raw	8	0.0168	0.9887	0.0123	0.994
	SNV	8	0.0137	0.9925	0.0101	0.9959
	SG (23,2,1) + SNV	8	0.0136	0.9926	0.0099	0.9961
	SNV + SG (15,2,1)	6	0.014	0.9921	0.0091	0.9967

Table 3. The performance parameters of PLS regression models for calibration, validation and prediction of VO adulteration in EVOO by different methods.

Datasets	LVs	$RMSE_C$	R^2_C	$RMSE_{CV}$	R^2_{CV}	$RMSE_P$	R^2_P
Video-1	5	0.0125	0.9937	0.0204	0.9834	0.0192	0.9853
Video-2	4	0.0203	0.9836	0.0237	0.9776	0.0204	0.9833
NIR	8	0.0152	0.9907	0.0263	0.9724	0.0245	0.9759
UV-Vis	8	0.0054	0.9988	0.0137	0.9925	0.0101	0.9959
Image-1	8	0.0175	0.9878	0.0336	0.9548	0.0288	0.9668
Image-2	8	0.0193	0.985	0.0357	0.9491	0.0258	0.9734

The calibration, validation and prediction results of PLS regression on all datasets have R^2 values greater than 0.94 and RMSE less than 0.04, as shown in Table 3. The optimal number of LVs for video data does not exceed 5, while that for other data is 8. To graphically visualize the quantification results of video, NIR, UV-Vis and image data, the predictions and the adulteration levels based on PLS regression models are plotted for validation and prediction, as shown in **Fig. S**6. For video datasets, the level of adulterant in EVOO is estimated with R^2_{CV} around 0.98 and the corresponding $RMSE_{CV}$ around 0.02. The obtained models, when applied to the prediction sets, are capable in predicting VO adulteration with similar results. The regression model based on NIR data gives a degraded performance in validation (R^2_{CV} = 0.9724 and $RMSE_{CV}$ = 0.0263) and prediction (R^2_P = 0.9759 and $RMSE_P$ = 0.0245) compared to the model based on video data. The most successful model is attained on UV-Vis data with robust statistical parameters (R^2_{CV} = 0.9925, $RMSE_{CV}$ = 0.0137, R^2_P = 0.9959 and $RMSE_P$ = 0.0101). For image datasets, the regression models obtain R^2_{CV} values lower than 0.955 with the corresponding $RMSE_{CV}$ higher than 0.03. Such models yield R^2_P below 0.975 and $RMSE_P$ above 0.025.

3.3. Variable selection

PLS regression model based on video data with full variables has proved the applicability of using smartphone videos for prediction of VO adulteration in EVOO. However, it could be difficult for the sensor system to be served as an efficient real-time system, because using smartphone to handle data with over hundreds of variables takes a long time and a high computational load. Therefore, an essential task to eliminate uninformative variables of video data is variable selection. Generally, the selection of important variables may not have much influence on the results, but have practical significance when developing real-time systems [25].

The statistical parameters of PLS regression on all datasets with variables selected by VIP are given in Table 4. Over half of the variables are removed with a threshold of 0.8, which cause a slight decrease in the overall performance of PLS models. For video data, R^2_P of 0.98 with corresponding $RMSE_P$ of 0.02 is achieved by VIP (>0.8) and PLS regression, which is close to the results based on the overall variables. Variable selection and PLS regression model based on UV-Vis data maintains a good performance with the highest R^2 values (>0.99) and the lowest RMSE (~0.01), while NIR and image data coupled with VIP and PLS regression reduce R^2 values by up to 0.027.

Table 4. The performance parameters of PLS regression on datasets using variables with VIP scores above the threshold value.

Datasets	LVs	$RMSE_C$	R^2_C	$RMSE_{CV}$	R^2_{CV}	$RMSE_P$	R^2_P	Threshold	No. variables
Video-1	5	0.0171	0.9884	0.0251	0.9749	0.0228	0.9792	0.8	208
Video-1	5	0.0248	0.9754	0.0382	0.9416	0.0481	0.9073	Frames: 89−109	42
Video-2	4	0.0213	0.9818	0.0248	0.9753	0.0215	0.9815	0.8	176
Video-2	6	0.0180	0.9871	0.0276	0.9695	0.0331	0.9562	Frames: 89−109	42
NIR	8	0.0153	0.9907	0.0288	0.9667	0.0275	0.9698	0.8	129
UV-Vis	8	0.0062	0.9985	0.013	0.9932	0.0103	0.9958	0.8	433
UV-Vis	4	0.013	0.9933	0.0147	0.9914	0.013	0.9933	3	7
Image-1	6	0.0245	0.976	0.0368	0.9459	0.0347	0.9518	0.8	60
Image-2	3	0.032	0.959	0.0449	0.9195	0.0433	0.925	0.8	40

The important variables of the two video datasets selected by VIP are depicted in Fig. 5a and b. These variables are in red and green colour channels in most cases. We merge all colour images appeared on the screen of smartphone into a colour spectrum, copy the colour spectrum for three times corresponding to the decomposed frames in RGB channels and display the obtained colour spectrum at the top of each subplot. The interval providing a good visualization of adulteration levels (see Fig. 2) usually has high VIP scores above 1.5, for example, interval 100−150 in red channel for set-a and interval 65−105 in green channel for set-b. A total of 121 variables are jointly selected for the two sets (intervals 5−21, 89−109 and 161−175 in red channel and 44−109 in green channel), which contain common frames 89−109. These frames have VIP scores around 1.5 and are corresponding to the screen colours varying from yellow to orange, as shown in Fig. 5c. PLS models based on the common frames can yield R^2 varying from 0.907 to 0.97 in validation and prediction.

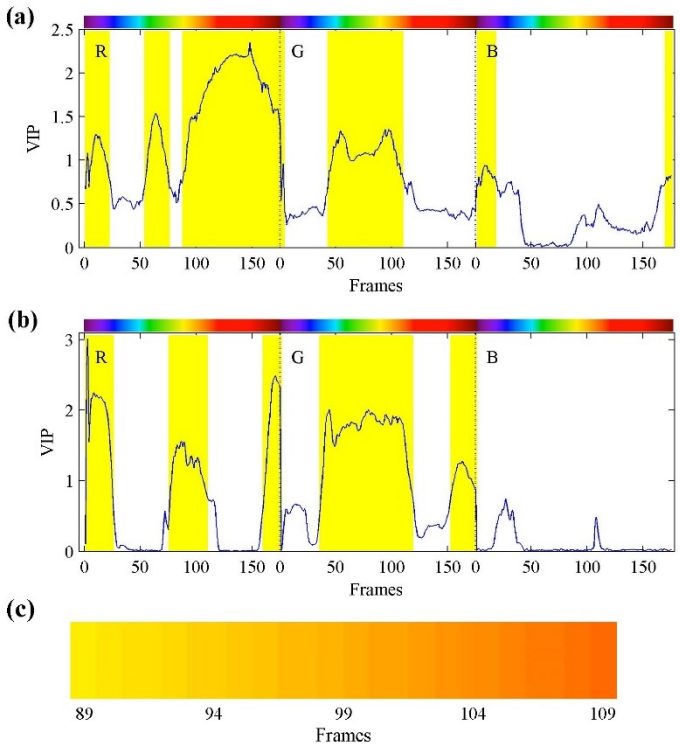

Fig. 5. Variable selection of two video datasets using VIP (a & b). The selected variables (VIP scores > 0.8) are highlighted in yellow. A colour spectrum of illumination corresponding to the variables is displayed at the top of each subplot. The screen colours of joint frames 89−109 are depicted in c.

Fig. 6 shows the VIP scores of UV-Vis data, with a visible colour spectrum corresponding to wavelengths 380−666 nm displayed at top. The VIP scores of wavelengths after 500 nm globally exceed that of wavelengths before 500 nm. We set the threshold of VIP to 3 and select wavelengths 592.7, 619, 614.6, 638.6, 526.6, 570.4 and 349.2 nm (VIP descending order) for modelling, yielding R^2_{CV} and R^2_P values above 0.99.

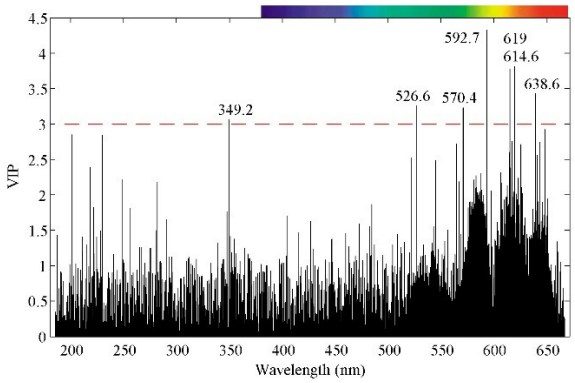

Fig. 6. Selection of important wavelengths using VIP (score > 3) on UV-Vis spectral data. A visible colour spectrum corresponding to wavelengths 380−666 nm is displayed at top.

3.4. Discussion

The sensor system based on smartphone videos and PLS regression effectively quantifies the minimum level of 5% VO adulteration in EVOO with R^2_P value higher than 98%. Although the quality of smartphone videos is not high, the regression results based on smartphone videos significantly outperforms those based on CVS by capturing colour spectral information. Such spectral information covers a narrow range of wavelengths with low spectral resolutions (~380−740 nm with ~2 nm intervals) compared to NIR (901−1721 nm with 1.65 nm intervals) and UV-Vis (186−666 nm with 1.5 nm intervals) used in experiments. However, the result of the sensor system is comparable to that of the baseline spectrometers. The colour spectrum of the sensor system covers the important wavelengths which provide useful information for PLS regression models to distinguish unadulterated and adulterated samples.

Our previous study captured smartphone videos under low-light conditions to reduce the influence of external light, while this study shows that PLS regression models based on the videos recorded under normal light and low-light conditions can yield similar results. Such a finding reduces the limitation of sampling conditions for the sensor system. However, a common problem of the sensor system as well as many other methods is that the constructed model cannot be used reliably under different measurement conditions. Therefore, it is necessary to control the intensity range of background light and to construct models capable of capturing sampling diversities.

4. Conclusions

In this work we use smartphone videos coupled with image processing and chemometrics to quantify the level of VO adulteration in EVOO. The actual and predicted values are highly consistent, yielding R^2 of 0.98 with the corresponding RMSE of 0.02. To compare the performance of the sensor system and baseline techniques, PLS regression models are constructed from UV-Vis, NIR and image data for the same task. The results demonstrate that the sensor system yields comparable performance to UV-Vis and NIR spectrometers, and outperforms CVS. Moreover, over half of the uninformative variables of these data are removed using VIP to improve the simplicity of models.

As the sensor system provides a low-cost solution for detecting and quantifying the adulteration in EVOO, it can be further developed into a real-time and online system to help consumers fight against food fraud. For example, sample videos are recorded via smartphone, uploaded to server and analysed by chemometrics models. However, there are still some technical barriers to overcome. In particular, the analysis of data measured under different conditions poses a challenge to the robustness and effectiveness of models. Our future work will optimize the sensor system for sampling, build large datasets and apply deep learning models for EVOO authentication and quality assessment.

Author contributions

W.H. proposed the sensor concept. V.J. developed the Android app. S.W. designed the experiments and analysed the data. S.Z. and V.J. performed the experiments. S.W. and S.Z. wrote the paper. W.H. and W.Z. reviewed the paper.

Acknowledgements

Financial support from Ulster University Global Challenges Fund (70642R) is gratefully acknowledged.

Reference

[1] J.L. Harwood, P. Yaqoob, U. Kingdom, H. Nutrition, U. Kingdom, Nutritional and health aspects of olive oil, Eur. J. Lipid Sci. Technol. 104 (2002) 685–697.

[2] U. Wahrburg, M. Kratz, P. Cullen, Mediterranean diet, olive oil and health, Eur. J. Lipid Sci. Technol. 104 (2002) 698–705. https://doi.org/10.1002/1438-9312(200210)104:9/10<698::AID-EJLT698>3.0.CO;2-A.

[3] G. Espadas-aldana, C. Vialle, J. Belaud, C. Vaca-garcia, C. Sablayrolles, Analysis and trends for Life Cycle Assessment of olive oil production, Sustain. Prod. Consum. 19 (2019) 216–230. https://doi.org/10.1016/j.spc.2019.04.003.

[4] R. Romaniello, A. Baiano, Discrimination of flavoured olive oil based on hyperspectral imaging, J. Food Sci. Technol. 55 (2018) 2429–2435. https://doi.org/10.1007/s13197-018-3160-8.

[5] H.W. Jiulin Shi, Dapeng Yuan, Shiguo Hao, Y.Z. , Ningning Luo, JuanLiu, Z.C. Weiwei Zhang, Xingdao He, J. Shi, D. Yuan, S. Hao, H. Wang, N. Luo, J. Liu, Y. Zhang, W. Zhang, X. He, Z. Chen, Stimulated Brillouin scattering in combination with visible absorption spectroscopy for authentication of vegetable oils and detection of olive oil adulteration, Spectrochim. Acta Part A Mol. Biomol. Spectrosc. 206 (2019) 8043–8050. https://doi.org/10.1016/j.saa.2018.08.031.

[6] F.J. Lara-Ortega, M. Beneito-Cambra, J. Robles-molina, J.F. García-reyes, B. Gilbert-López, A. Molina-Díaz, Direct olive oil analysis by mass spectrometry: A comparison of different ambient ionization methods, Talanta. 180 (2018) 168–175. https://doi.org/10.1016/j.talanta.2017.12.027.

[7] L. D.-S., N. B.-S., B. S.-Y., K. K., Characterization of fatty acids composition in vegetable oils by gas chromatography and chemometrics, Anal. Chim. Acta. 358 (1998) 163–175.

[8] G. Vlahov, 13C nuclear magnetic resonance spectroscopy to determine olive oil grades, Anal. Chim. Acta. 577 (2006) 281–287. https://doi.org/10.1016/j.aca.2006.06.044.

[9] J.A. Cayuela-Sánchez, J. Palarea-Albaladejo, J.F. García-Martín, M. del C. Pérez-Camino, Olive oil nutritional labeling by using Vis/NIR spectroscopy and compositional statistical methods, Innov. Food Sci. Emerg. Technol. 51 (2019) 139–147. https://doi.org/10.1016/j.ifset.2018.05.018.

[10] M. Ferreiro-González, G.F. Barbero, J.A. Álvarez, A. Ruiz, M. Palma, J. Ayuso, Authentication of virgin olive oil by a novel curve resolution approach combined with visible spectroscopy, Food Chem. 220 (2017) 331–336.

https://doi.org/10.1016/j.foodchem.2016.10.015.

[11] H. Ali, M. Saleem, M.R. Anser, S. Khan, R. Ullah, M. Bilal, Validation of Fluorescence Spectroscopy to Detect Adulteration of Edible Oil in Extra Virgin Olive Oil (EVOO) by Applying Chemometrics, Appl. Spectrosc. 72 (2018) 1371–1379. https://doi.org/10.1177/0003702818768485.

[12] A. Sayago, R. González-Domínguez, R. Beltrán, Á. Fernández-Recamales, Combination of complementary data mining methods for geographical characterization of extra virgin olive oils based on mineral composition, Food Chem. 261 (2018) 42–50. https://doi.org/10.1016/j.foodchem.2018.04.019.

[13] W. Dong, Y. Zhang, B. Zhang, X. Wang, Quantitative analysis of adulteration of extra virgin olive oil using Raman spectroscopy improved by Bayesian framework least squares support vector machines, Anal. Methods. 4 (2012) 2772–2777. https://doi.org/10.1039/c2ay25431j.

[14] C. Ruiz-Samblás, F. Marini, L. Cuadros-Rodríguez, A. González-Casado, Quantification of blending of olive oils and edible vegetable oils by triacylglycerol fingerprint gas chromatography and chemometric tools, J. Chromatogr. B Anal. Technol. Biomed. Life Sci. 910 (2012) 71–77. https://doi.org/10.1016/j.jchromb.2012.01.026.

[15] D. Wu, D.W. Sun, Colour measurements by computer vision for food quality control - A review, Trends Food Sci. Technol. 29 (2013) 5–20. https://doi.org/10.1016/j.tifs.2012.08.004.

[16] K.D.T.M. Milanez, M.J.C. Pontes, Classification of edible vegetable oil using digital image and pattern recognition techniques, Microchem. J. 113 (2014) 10–16. https://doi.org/10.1016/j.microc.2013.10.011.

[17] SCiO - The World's First Pocket Sized Molecular Sensor, (n.d.). https://www.consumerphysics.com/.

[18] Tellspec – Analysis, Food Safety, Food Database, Food Security, (n.d.). http://tellspec.com/.

[19] N. Karagiorgos, N. Nenadis, D. Trypidis, K. Siozios, S. Siskos, S. Nikolaidis, M.Z. Tsimidou, An approach for estimating adulteration of virgin olive oil with soybean oil using image analysis, 2017 6th Int. Conf. Mod. Circuits Syst. Technol. MOCAST 2017. (2017). https://doi.org/10.1109/MOCAST.2017.7937672.

[20] W. Song, N. Jiang, H. Wang, J. Vincent, Use of smartphone videos and pattern recognition for food authentication, Sensors Actuators, B Chem. 304 (2020) 127247. https://doi.org/10.1016/j.snb.2019.127247.

[21] R.D. Snee, Validation of Regression Models: Methods and Examples, Technometrics. 19 (1977) 415–428. https://doi.org/10.1080/00401706.1977.10489581.

[22] H. WOLD, Nonlinear Iterative Partial Least Squares (NIPALS) Modelling: Some Current Developments, in: Multivar. Anal., 1973: pp. 383–407. https://doi.org/10.1016/B978-0-12-426653-7.50032-6.

[23] S. Wold, E. Johansson, M. Cocchi, PLS - partial least-squares projections to latent structures., in: 3D QSAR Drug Des., 1993.

[24] M. Mathea, W. Klingspohn, K. Baumann, Chemoinformatic Classification Methods and their Applicability Domain, Mol. Inform. 35 (2016) 160–180. https://doi.org/10.1002/minf.201501019.

[25] M. Kamruzzaman, Y. Makino, S. Oshita, Rapid and non-destructive detection of chicken adulteration in minced beef using visible near-infrared hyperspectral imaging and machine learning, J. Food Eng. 170 (2016) 8–15. https://doi.org/10.1016/j.jfoodeng.2015.08.023.